

# Velocity feedback for controlling vertical vibrations of pedestrian-bridge crossing. Practical guidelines

Xidong Wang<sup>\*1</sup>, Emiliano Pereira<sup>2</sup>, Iván M. Díaz<sup>1</sup> and Jaime H. García-Palacios<sup>1</sup>

<sup>1</sup>E.T.S. Ingenieros de Caminos, Canales y Puertos, Universidad Politécnica de Madrid, Calle del Profesor Aranguren 3, Madrid, Spain  
<sup>2</sup>Department of Signal Processing and Communications, Universidad de Alcalá, Alcalá de Henares (Madrid), Spain

(Received November 6, 2017, Revised March 30, 2018, Accepted April 3, 2018)

**Abstract.** Active vibration control via inertial mass actuators has been shown as an effective tool to significantly reduce human-induced vertical vibrations, allowing structures to satisfy vibration serviceability limits. However, a lot of practical obstacles have to be solved before experimental implementations. This has motivated simple control techniques, such as direct velocity feedback control (DVFC), which is implemented in practice by integrating the signal of an accelerometer with a band-pass filter working as a lossy integrator. This work provides practical guidelines for the tuning of DVFC considering the damping performance, inertial mass actuator limitations, such as stroke and force saturation, as well as the stability margins of the closed-loop system. Experimental results on a full scale steel-concrete composite structure (behaves similar to a footbridge) with adjustable span are reported to illustrate the main conclusions of this work.

**Keywords:** active control; human-induced vibrations; band-pass filter; direct velocity feedback control; inertial mass actuator

## 1. Introduction

Improvements in design and construction have led to light and slender structures that have increased susceptibility to vibrations. These structures satisfy ultimate limit state criteria but have the potential of attracting complaints coming from vibrations due to human induced loading (HIL) (Hanagan 2005, Moutinho *et al.* 2011, Lu *et al.* 2012), or due to wind-induced loading (Bortoluzzi *et al.* 2015). Passive control using tuned mass dampers (Casado *et al.* 2013) is the most common solution adopted for HIL vibration problems (Casati 2016, Casati *et al.* 2017) in footbridges, allowing structures to satisfy vibration serviceability limits. Semi-active control strategies for HIL have been also studied intensively in order to enhance control robustness under system changes (Soria *et al.* 2017, Nagarajaiah and Jung, 2014). However, active vibration control (AVC) via inertial mass actuators has been shown to be more effective to significantly reduce the level of HIL vibration response (Casado *et al.* 2013), being also robust to system changes.

The use of inertial mass actuators to implement AVC is a relatively new research area in civil engineering, so a lot of obstacles have to be overcome before this field can fully mature. These actuators can exert forces in one particular direction, which is usually vertical in HIL control implementations. However, application of the control force, which is similar to adding energy to the structure, can make the closed control loop unstable. This instability is mainly

due to the fact that the linear and nonlinear model of the actuator is not well considered in the controller design (Hudson and Reynolds 2012, Teng *et al.* 2014). Hudson and Reynolds (2012), Teng *et al.* (2014) and Alujevic *et al.* (2014) concludes that the resonance frequency of the inertial mass actuator should be as low as practically possible in order to simplify the controller design (the actuator low-frequency dynamic response can thus be avoided). However, a suitable actuator cannot always be obtained in practice.

Different control strategies have been proposed in order to mitigate the aforementioned problems. An important group of strategies try to implement direct velocity feedback control (DVFC). For example, in (Díaz and Reynolds 2009), a feed-through term between the structure acceleration and actuator force is combined with an ideal integration of the modified structure output. Other option, which was proposed in (Díaz and Reynolds 2010), is to combine an acceleration feedback with a phase-lag compensator and a high-pass filter. This controller is like an integral action in the bandwidth of interest, which is robust to stroke saturation due to the high-pass filter. The stability margins of the controller proposed in (Díaz and Reynolds 2009) is improved in (Díaz *et al.* 2012a) by an approximate inversion of the actuator dynamics, allowing the application of integral resonant control theory (Aphale *et al.* 2007).

Other control strategies try to custom the actuator dynamics. For example, an inner control loop is proposed in (Díaz *et al.* 2012b). Other examples are (Zilletti *et al.* 2014, Zilletti 2016), in which an inerter added to an AVC system can reduce the natural frequency of the inertial mass actuator, improving the stability of the feedback loop and thus its performance. Finally, more complex control strategies also have been proposed. For example, the

\*Corresponding author, Ph.D. Student  
E-mail: wangxidong@caminos.upm.es

variable gain feedback control strategy (Teng *et al.* 2014, Xu *et al.* 2014) and time delay control algorithm (Jang *et al.* 2015) are analyzed and adopted to make the active mass damper (AMD) system more robust and more adaptive to excitation intensity variations. Other examples, such as the multi-loop vibration controller, disturbance observer introduced into an outer-loop DVFC controller and other dynamic compensators, are investigated in recent researches (Nyawako *et al.* 2016, Nyawako *et al.* 2015, Ubaid *et al.* 2015). However, these features and new control components undoubtedly complicate the practical implementation and its likelihood of success.

Simple and easy to tune control laws are more suitable to be implemented in practice than complex ones. Thus, works like (Pereira and Aphale 2013) try to propose simple design guides when practical issues must be considered. Special attention to (Hudson *et al.* 2016) should be paid for AVC of human-induced vibrations. This work considers a generalized system and investigates what sort of performance can be achieved theoretically by an ideal DVFC system. In addition, it considers the added complexity of actuator dynamics to demonstrate how this degrades the performance from optimal, assuming a fixed value of cut-off frequency of the band-pass filter (used to implement the DVFC).

The work presented herein extends the results and conclusions of (Hudson *et al.* 2016) and provides interesting and simple design rules for future implementing. As in (Hudson *et al.* 2016), the model is considered as a linear second order model (i.e., the model only considered the most important vibration mode), where the control objective is to design the optimum DVFC in terms of maximum damping. It should be noted that it is assumed that the fundamental vibration mode is in the bandwidth of interests. In other words, it is not necessary to consider a HIL model to design the controller.

The main contribution of this work is the study of the relationships between the maximum damping performance as a function of frequency ratios between actuator, structure and high-pass filter. In addition, this work also relates the actuator stroke and the actuator force with the gain margin and actuator damping ratio in order to avoid stroke and force saturation. All these theoretical studies are summarized into a practical guideline for the selection of a proper value of the cut-off frequency of the band-pass filter which considers the control performance together with the maximum stroke and force of the actuator. In other words, this paper concludes that the cut-off frequency of the band-pass filter must also be considered as a control parameter, which can improve the control performance for a certain frequency ratio of the fundamental vibration mode of the structure to the actuator.

The practical guidelines together with the assumed simplifications are illustrated by showing simulation and experimental results. These results are obtained on a full scale steel-concrete composite structure (behaves similar to a footbridge) with adjustable span, which has a configurable fundamental vibration mode. The experimental results also shows that the second order model simplification can be assumed in practice.

This paper is organized as follows. Section 2 briefly explains the ideal DVFC. In section 3, practical guidelines for the design are presented together with a complete demonstration of these. Section 4 details the experimental work, including the dynamic identification of a full-scale laboratory structure, the AVC implementation, and frequency response tests. Finally, the main conclusions are given in Section 5.

## 2. Ideal velocity feedback control

A simplified scheme for AVC based on velocity feedback is shown in Fig. 1. The dynamics of the structure, inertial mass actuator and the controller are represented by  $G$ ,  $G_A$  and  $C$ , respectively.

The structure is assumed as a single degree of freedom (SDOF), considering the fundamental vibration mode. Thus, the frequency response function (FRF) between the acceleration and the force of the bare structure is as follows:

$$G(j\omega) = \frac{(-1/m_1)\omega^2}{(\omega_1^2 - \omega^2) + j \cdot 2\xi_1\omega_1 \cdot \omega} \quad (1)$$

$\omega$  being the angular frequency,  $m_1$ ,  $\xi_1$  and  $\omega_1$  are the modal participation factor, damping ratio and natural frequency of the fundamental vibration mode, respectively.

If  $G_A = K_A$  is constant, i.e., no dynamics from the actuator are introduced (ideal actuator), and  $C(j\omega) = K_C/(j\omega)$  is a pure integrator with infinity magnitude response at zero frequency, the FRF of the closed loop system can be obtained from Fig. 1 as follows

$$G_{CL}(j\omega) = \frac{a}{f_E} = \frac{(-1/m_1)\omega^2}{(\omega_1^2 - \omega^2) + j(2\xi_1\omega_1 + K_C K_A/m_1)\omega} \quad (2)$$

in which  $a$  is the acceleration of the structure and  $f_E$  is the excitation force to the structure. In an ideal DVFC control, the added damping to the structure is proportional to  $K_C K_A$ .

## 3. Modified velocity feedback control

### 3.1 Practical considerations

Ideal DVFC is not implementable since there exists a lot of practical issues to be considered, such as the off-set values in the accelerometers' measurement, actuator low-frequency response and spillover effect (i.e., instability due to non-modeled high frequency dynamics).

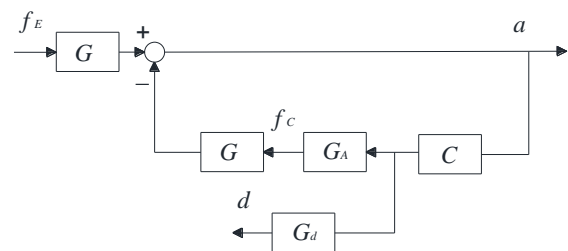


Fig. 1 General scheme of AVC

The inertial mass actuator model used in this paper is an APS Dynamics model 400 electrodynamic actuator, whose FRF can be written as (Preumont 2011)

$$G_A(j\omega) = \frac{-K_A\omega^2}{(\omega_A^2 - \omega^2) + j \cdot 2\xi_A\omega_A \cdot \omega} \quad (3)$$

in which  $\xi_A$ ,  $\omega_A$  are the damping ratio and frequency of the actuator respectively. A real signal acquired from accelerometers has off-set. Then, the ideal integrator must be replaced by a band-pass filter (i.e., a combination of an ideal integration and a high-pass filter) in order to obtain the velocity from acceleration. In addition, a low-pass filter may be required to guarantee the finite gain property of the control loop at high frequencies, avoiding spillover problems (Griggs *et al.* 2007). The FRF of both filters can be written together as follows (Hudson *et al.* 2016)

$$C(j\omega) = \frac{jK_C\omega}{(\omega_{HP}^2 - \omega^2) + j \cdot 2\omega/\sqrt{2} \cdot \omega_{HP}} \cdot \frac{\omega_{LP}^2}{(\omega_{LP}^2 - \omega^2) + j \cdot 2\omega/\sqrt{2} \cdot \omega_{LP}} \quad (4)$$

in which the cut-off frequency of the second order Butterworth band-pass and low-pass filters are  $\omega_{HP}$  and  $\omega_{LP}$ , respectively. The band-pass filter mitigates the problem resulted from the signal low-frequency components, alleviating the actuator stroke saturation problem. In addition, the low-pass filter can reduce the high-frequency gain in order to guarantee the stability of the system.

### 3.2 Non-dimensional study

The objective of this section is to show the best attenuation level that can be achieved with the control scheme of Fig. 1 as a function of the ratio of the actuator frequency to the structure natural frequency. This is defined as  $r_A = \omega_A/\omega_1$ , and the ratio of the cut-off frequency of the lossy integrator (or band-pass filter) to the structure natural frequency, defined as  $r_{HP} = \omega_{HP}/\omega_1$ . In addition, the value of the stroke and force gains (i.e., the magnitude of the transfer functions (TFs) between  $d$  and  $f_E$  and between  $f_C$  and  $f_E$ , respectively) are analyzed. This analysis shows that there is a tradeoff between the attenuation performance and the maximum stroke and force values.

First of all, the non-dimensional FRF of the structure defined in Eq. (1) is defined as follows

$$G(j\hat{\omega}) = \frac{(-1/m_1)\hat{\omega}^2}{(1 - \hat{\omega}^2) + j \cdot 2\xi_1 \cdot \hat{\omega}} \quad (5)$$

$\hat{\omega}$  being equal to  $\omega/\omega_1$ . If  $\hat{\omega}$  and  $r_A$  are considered, the non-dimensional FRF of the actuator defined in Eq. (3) is as follows

$$G_A(j\hat{\omega}) = \frac{-K_A\hat{\omega}^2}{(r_A^2 - \hat{\omega}^2) + j \cdot 2\xi_A r_A \cdot \hat{\omega}} \quad (6)$$

The mass displacement can be obtained by integrating twice the mass acceleration, which is obtained by dividing the force by  $m_A$ . Thus, the FRF between the actuator mass

( $m_A$ ) displacement and the control signal is as follows

$$G_d(j\hat{\omega}) = \frac{G_A(j\hat{\omega})}{m_A\hat{\omega}^2} \quad (7)$$

Finally, the non-dimensional FRF of the controller defined in Eq. (4) is as follows

$$C(j\hat{\omega}) = \frac{jK_C\hat{\omega}}{(r_{HP}^2 - \hat{\omega}^2) + j \cdot 2r_{HP}/\sqrt{2} \cdot \hat{\omega}} \cdot \frac{r_{LP}^2}{(r_{LP}^2 - \hat{\omega}^2) + j \cdot 2r_{LP}/\sqrt{2} \cdot \hat{\omega}} \quad (8)$$

$r_{LP}$  being equal to  $\omega_{LP}/\omega_1$ .

The attenuation performance is defined in terms of infinity norm (i.e., the maximum of the FRF-magnitude) reduction, which can be written as follows

$$\text{Attenuation (dB)} = -20 \log_{10} \frac{\|G_{a,f_E}\|_{\infty}}{\|G\|_{\infty}} \quad (9)$$

in which  $\|G_{a,f_E}\|_{\infty}$  and  $\|G\|_{\infty}$  are the  $H_{\infty}$  norm of the closed-loop and open-loop systems, respectively. The value of  $\|G\|_{\infty}$  can be considered, when the flexible structure has a small damping ratio, as follows (Ogata 2010)

$$\|G\|_{\infty} = \frac{1/m_1}{2\xi_1\sqrt{1 - \xi_1^2}} \cong \frac{1}{2\xi_1 m_1} \quad (10)$$

Then, if Eqs. (5), (6) and (8) are considered, the closed-loop system FRF is obtained as follows

$$G_{a,f_E}(j\hat{\omega}) = \frac{G(j\hat{\omega})}{1 + G(j\hat{\omega}) \cdot G_A(j\hat{\omega}) \cdot C(j\hat{\omega})} = \frac{-(\hat{\omega}^2/m_1) \cdot D_{G_A}(j\hat{\omega}) \cdot D_C(j\hat{\omega})}{D_G(j\hat{\omega}) \cdot D_{G_A}(j\hat{\omega}) \cdot D_C(j\hat{\omega}) + j\hat{\omega}^5 \tilde{K}_C} \quad (11)$$

in which the normalized control gain is  $\tilde{K}_C = (r_{LP}^2 K_A K_C)/m_1$  and the variables  $D_G(j\hat{\omega})$ ,  $D_{G_A}(j\hat{\omega})$  and  $D_C(j\hat{\omega})$  are, respectively, the denominators of Eqs. (5), (6) and (8). Then, if Eqs. (10) and (11) are considered, the attenuation level defined in Eq. (9) becomes

$$\text{Attenuation (dB)} = -20 \log_{10} \left\| \frac{-(2\xi_1\hat{\omega}^2)D_{G_A}(j\hat{\omega}) \cdot D_C(j\hat{\omega})}{D_G(j\hat{\omega}) \cdot D_{G_A}(j\hat{\omega}) \cdot D_C(j\hat{\omega}) + j\hat{\omega}^5 \tilde{K}_C} \right\|_{\infty} \quad (12)$$

The controller design consists of maximizing Eq. (12) for given values of  $r_{LP}$ ,  $r_{HP}$  and gain margin of the closed-loop system. Each design is obtained by calculating the optimum value of  $\tilde{K}_C$  with the scalar bounded nonlinear function minimization *fminbnd* of MATLAB. The boundary conditions used in *fminbnd* are  $\tilde{K}_C = 0$  and  $\tilde{K}_C$  equal to the gain margin of  $G(j\hat{\omega})G_A(j\hat{\omega})C(j\hat{\omega})/\tilde{K}_C$  (see Eq. (12)), which is obtained by *margin* command of MATLAB, divided by the given gain margin value.

Fig. 2 shows the attenuation level defined in Eq. (12) when  $\xi_A = 0.3$ . The upper limit value of  $\tilde{K}_C$  is equal to the gain margin of  $G(j\hat{\omega})G_A(j\hat{\omega})C(j\hat{\omega})/\tilde{K}_C$  divided by one (0 dB gain margin), two (6 dB gain margin) and four (12 dB

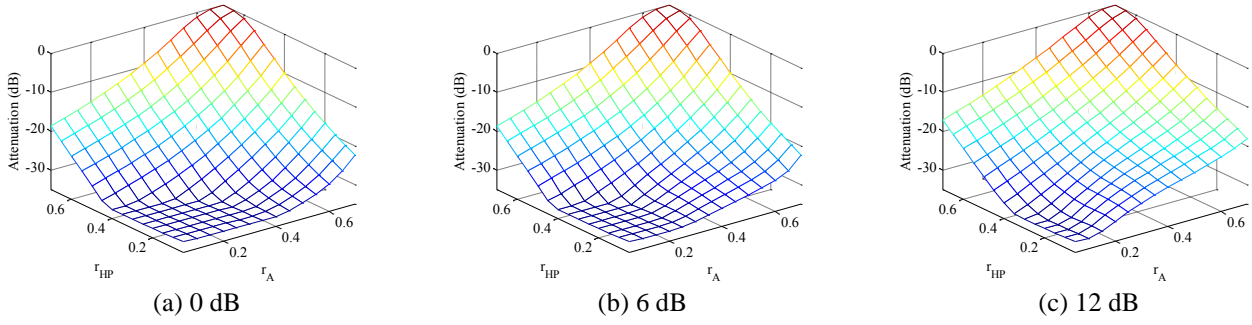


Fig. 2 Attenuation (dB) when the actuator damping is equal to 0.3, and the upper limit of  $\hat{K}_C$  guarantees a minimum gain margin

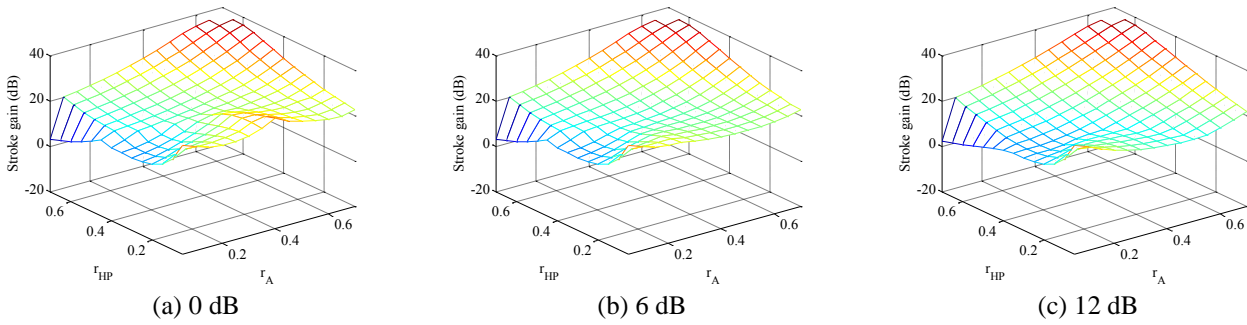


Fig. 3 Stroke gain (dB) when the actuator damping is equal to 0.3, and the upper limit of  $\hat{K}_C$  guarantees a minimum gain margin

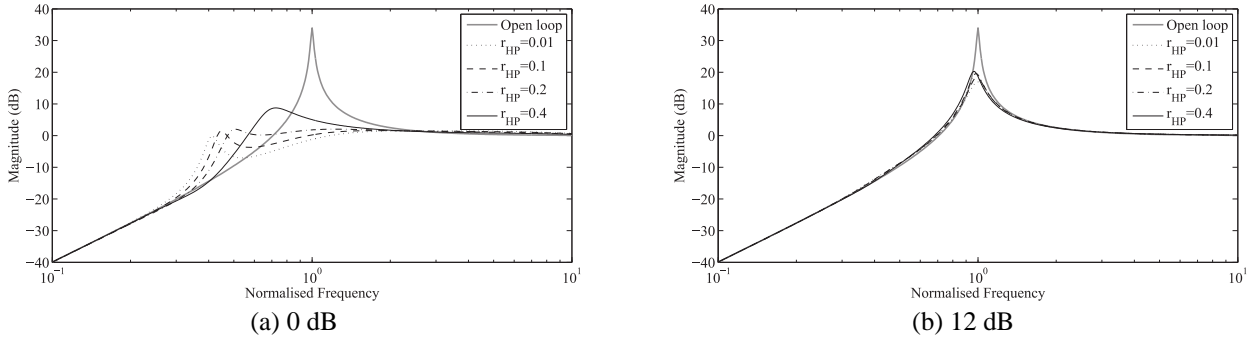


Fig. 4 Influence of  $r_{HP}$  on the attenuation (dB) when the actuator damping is equal to 0.3,  $r_A = 0.4$ , and the upper limit of  $\hat{K}_C$  guarantees a minimum gain margin.

gain margin). Note that there is set of values of  $r_{HP}$  and  $r_A$  for which the maximum damping performance is achieved (approximately equal to -32 dB). Then, there are values of  $r_A$  for which the attenuation performance is deteriorated (i.e., the maximum damping is not achieved). The range of values of  $r_A$  is smaller when the gain margin restriction is increased, a significant attenuation can be obtained for the three gain margin restriction examples. Thus, if an attenuation level of 20 dB is considered as a very good control performance in AVC applications, this can be obtained when  $r_A < 0.7$  for a gain margin of 6 dB and when  $r_A < 0.6$  for a gain margin of 12 dB.

If a 20 dB attenuation level can be achieved, the next question should be what the most convenient implementation is. In order to illustrate this issue, the stroke and force gain are also plotted. The FRF between the actuator stroke and the excitation can be defined as follows

$$G_{d,f_E}(j\hat{\omega}) = \frac{-j\hat{\omega}^3 \hat{K}_C / m_A}{D_C(j\hat{\omega}) \cdot D_{G_A}(j\hat{\omega}) \cdot D_C(j\hat{\omega}) + j\hat{\omega}^5 \hat{K}_C} \quad (13)$$

Fig. 3 shows the stroke gain defined as follows

$$\text{Stroke Gain (dB)} = 20 \log_{10} \|G_{d,f_E}(j\hat{\omega})\|_{\infty} \quad (14)$$

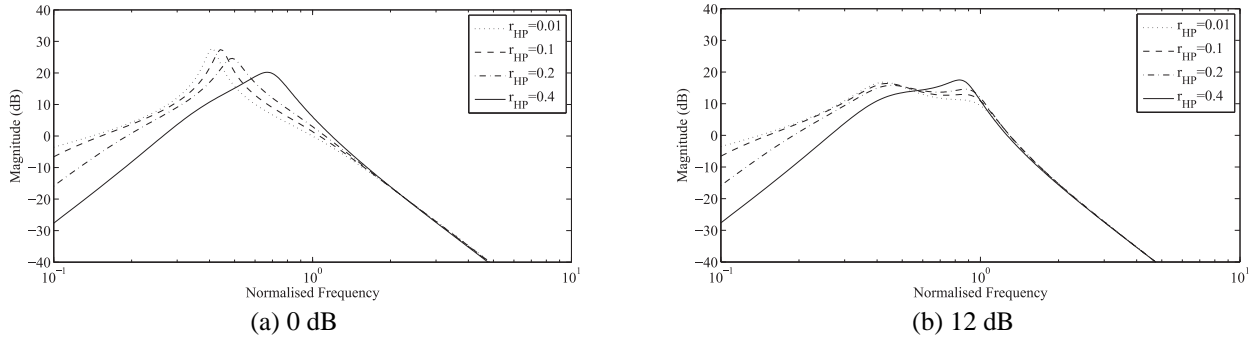


Fig. 5 Influence of  $r_{HP}$  on the stroke gain (dB) when the actuator damping is equal to 0.3,  $r_A = 0.4$ , and the upper limit of  $\hat{K}_C$  guarantees a minimum gain margin

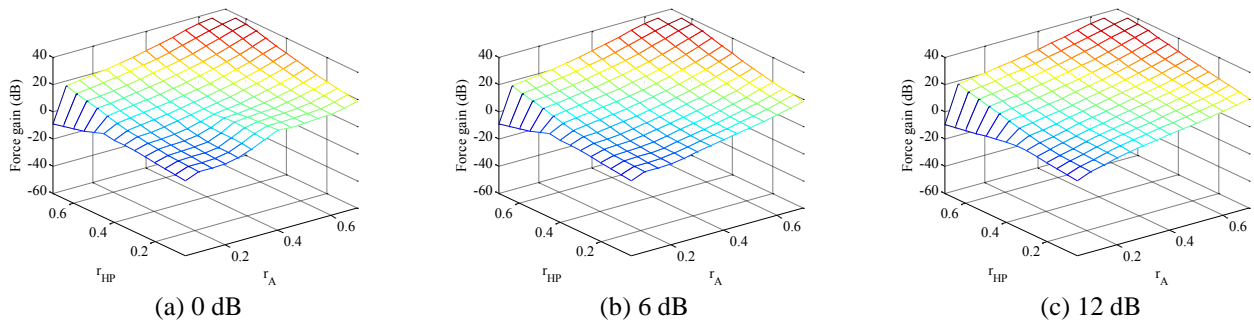


Fig. 6 Force gain (dB) when the actuator damping is equal to 0.3, and the upper limit of  $\hat{K}_C$  guarantees a minimum gain margin

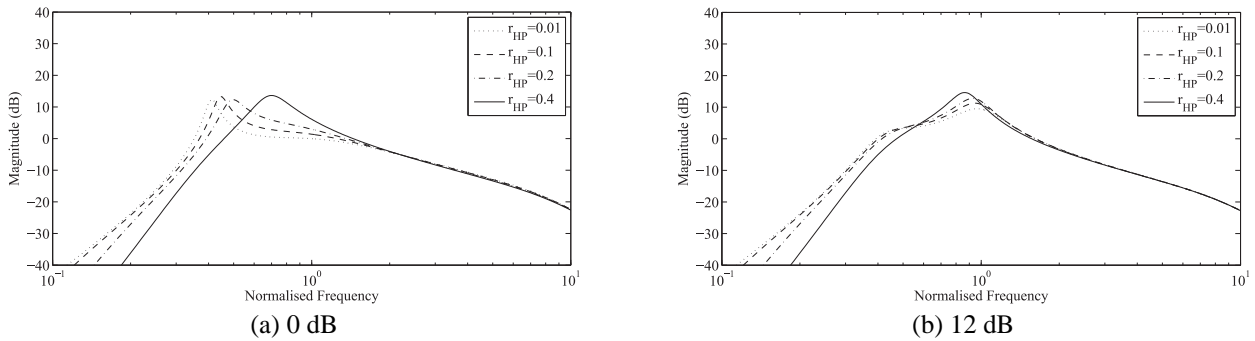


Fig. 7 Influence of  $r_{HP}$  on the force gain (dB) when the actuator damping is equal to 0.3,  $r_A = 0.4$ , and the upper limit of  $\hat{K}_C$  guarantees a minimum gain margin

assuming the following actuator parameters:  $m_A = 1$  and  $\xi_A = 0.3$ . Note that the value of  $m_A = 1$  is not relevant to show that the actuator stroke gain: i) is reduced when the gain margin is increased, which could be obvious since the damping performance is deteriorated, and ii) depends on  $r_{HP}$ , having its minimum value around  $r_{HP} = 0.4$  for small values of  $r_A$ .

This is better illustrated in Figs. 4 and 5, where the attenuation and the stroke FRF are plotted for  $\xi_A = 0.3$  and  $r_A = 0.4$ . Note that for a gain margin equal to 0 dB, the increment of  $r_{HP}$  reduces the actuator stroke gain, and the most important fact is that the maximum actuator

displacement occurs at the frequency close to the natural frequency of the structure ( $r_{HP} = 0.4$ ). This is because the closed-loop poles of the actuator have small damping ratios when  $r_{HP}$  is not high enough, which might cause problems if there is a perturbation close to actuator frequency. In addition, the problem of stroke gain is less important when the gain margin is 12 dB, where the actuator displacement is approximately constant in the bandwidth of interest (Fig. 5(b)). However, although the damping performance (attenuation close to 20 dB) is worse than 0 dB-gain margin case, it will impart significant damping for practical implementation.

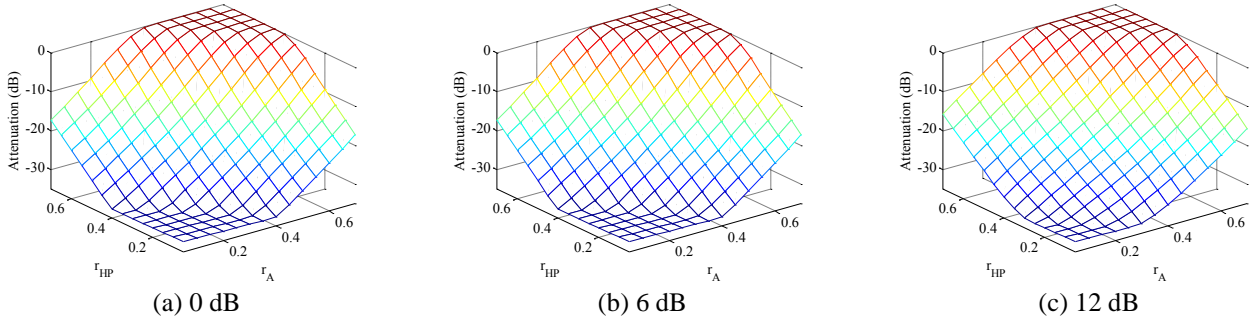


Fig. 8 Attenuation (dB) when the actuator damping is equal to 0.7, and the upper limit of  $\tilde{K}_C$  guarantees a minimum gain margin

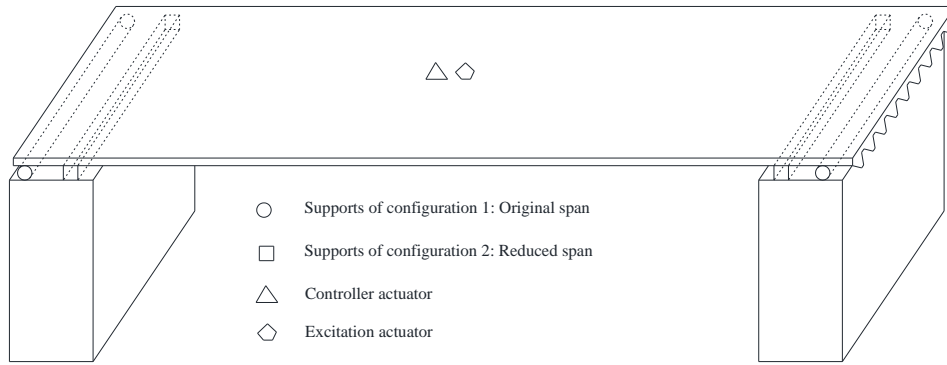


Fig. 9 Experimental setup configurations

The actuator force gain should be also studied. The FRF between the actuator force and excitation force can be defined as follows

$$G_{f_C, f_E}(j\hat{\omega}) = \frac{j\hat{\omega}^5 \tilde{K}_C}{D_G(j\hat{\omega}) \cdot D_{G_A}(j\hat{\omega}) \cdot D_C(j\hat{\omega}) + j\hat{\omega}^5 \tilde{K}_C} \quad (15)$$

Fig. 6 shows the force gain defined as follows

$$\text{Force Gain (dB)} = 20 \log_{10} \|G_{f_C, f_E}(j\hat{\omega})\|_{\infty} \quad (16)$$

in which  $\xi_A = 0.3$ . It can be observed that force is reduced in an interval of  $r_A$  when the gain margin is increased (around  $r_A=0.4$ ). However, this issue is better illustrated in Fig. 7, where it can be seen that the control force focuses on the natural frequency of the structure. It explains why an attenuation performance around 20 dB can be obtained with a gain margin of 12 dB. Therefore, the conclusion of this study, from the practical implementation point of view, is that a proper gain margin should: i) improve the relative stability of the system, ii) optimize the actuator behavior into the natural frequency of the structure, and iii) the damping performance is kept into the advisable levels. In addition, it also shows that a small value of  $r_{HP}$  is not always recommended since it increases the stroke gain and does not focus on the natural frequency of the structure. Finally, it is shown herein the influence of the actuator damping into the damping performance. Fig. 8 shows the attenuation (dB) when the actuator damping is equal to 0.7.

It can be seen that the influence of actuator damping deteriorates the attenuation performance for high values of  $r_A$  as compared with Fig. 2. Therefore, the increment of actuator damping may be not advisable if  $r_A$  is sufficiently high.

### 3.3 Design guidelines

Based on the above non-dimensional study, the following design process is proposed:

- (i) Identify the structure and actuator dynamics.
- (ii) Calculate the value of  $r_A$ .
- (iii) If  $r_A \leq 0.6$ , fix a gain margin of 12 dB in order to obtain the control gain for a set of values  $r_{HP}$  between 0.1 and 0.4.
- (iv) Test the control gain for  $r_{HP} = 0.4$  under the most unfavorable perturbation in order to check the maximum level of vibration and actuator mass displacement.
- (v) If the maximum actuator mass displacement is small enough (i.e., sufficiently safe), the value of  $r_{HP} = 0.4$  can be reduced.
- (vi) If the maximum vibration level is not achieved, repeat (iii)-(v) for a smaller gain margin.

Note that it is not convenient to reduce the gain margin below 6 dB since the closed-loop system might be unstable due to the unmodeled dynamics.

#### 4. Experimental implementation

To illustrate the viability of design guidelines for a modified velocity feedback, experimental tests are carried out on a light-weight structure (shown in Fig. 9). This is a steel-concrete composite slab, with a dimension of 5.8 m  $\times$  1.8 m and a maximum depth of only 14 cm. The structure is simply supported and behaves similar to a pedestrian bridge. The supports can be moved to change the fundamental vibration mode frequency of the structure.

The experiment is carried out with two APS Dynamics electrodynamic actuators: one is to excite vibration of the structure (model 144), and the other is to control the vibration (model 400). They are placed at almost the same point (i.e., at the midpoint of the mid span (Fig. 10)).

First of all, the experimental identification of the structure is carried out by measuring the force exerted by the actuator and the acceleration of the structure. The excitation (vertical forces) is configured as a chirp signal from 0 Hz to 30 Hz with a duration of 1800 seconds. In Fig. 11(a), it can be seen the comparison between the FRF measured and the identified model of two different configurations. Configuration 1 has  $m_1 = 1400 \text{ kg}$ ,  $\omega_1 = 2\pi \cdot 5.5 \text{ rad/s}$  and  $\xi_1 = 0.01$ ; configuration 2 has  $m_1 = 1400 \text{ kg}$ ,  $\omega_1 = 2\pi \cdot 6.6 \text{ rad/s}$  and  $\xi_1 = 0.01$ . In addition, using the aforementioned chirp signal, by estimating the TF between actuator force (acceleration of the actuator multiplied by  $m_A$ ) and the chirp signal, the identified modal parameters of APS Dynamics model 400 electrodynamic actuator are obtained (see Fig. 11(b)):  $\omega_A = 2\pi \cdot 2.7 \text{ rad/s}$ ,  $\xi_A = 0.25$ ,  $K_A = 230 \text{ N/V}$  and  $\epsilon = 14$ . The term  $\epsilon$  models the high-frequency dynamics of the actuator, which can be represented as follows:

$$G_A(j\omega) = \frac{-K_A \omega^2}{-\omega^2 + 2j\xi_A r_A \omega_1 \omega + r_A^2 \omega_1^2} \cdot \frac{2\pi\epsilon}{j\omega + 2\pi\epsilon} \quad (17)$$

in which  $r_A$  is equal to 0.41 and 0.49 for configuration 1 and 2, respectively.

This dynamics must be inverted (i.e., compensated) to apply the theory described in Section 3.2. Thus, the Eq. (8) is changed by the following

$$C_\epsilon(j\hat{\omega}) = C(j\omega) \cdot \frac{j\hat{\omega} + 2\pi\epsilon/\omega_1}{2\pi\epsilon} \quad (18)$$

Then, the practical guidelines of Section 3.3 are followed, where  $r_{LP} = 10$  and a gain margin of 12 dB are considered for configuration 1. Four different values of  $r_{HP}$  are taken into account in order to show the differences between them in terms of attenuation. Fig. 12(a) shows the simulation FRFs corresponding to the values of  $r_{HP} \in \{0.1, 0.2, 0.3, 0.4\}$ . Fig. 12(b) shows the comparison between experimental and simulated results when  $r_{HP} = 0.2$ . It should be remarked that an attenuation of 20 dB can be achieved with a gain margin of 12 dB. Finally, it should be noted that the maximum stroke was kept below 2.8 cm when a chirp signal from 2 Hz to 9 Hz with a duration of 600 seconds was used as excitation. Then, a gain margin of 12 dB might be used.

The same optimal design, where  $r_{LP} = 10$  and a gain margin of 6 dB are taken into account for configuration 2. Four different values of  $r_{HP}$  are considered in order to show the differences between them in terms of attenuation. Figure 13(a) shows the simulated FRFs corresponding to the values of  $r_{HP} \in \{0.1, 0.2, 0.3, 0.4\}$ . Fig. 13(b) shows the comparison between experimental and simulation results when  $r_{HP} = 0.4$ . It should be remarked that an attenuation of 26 dB can be achieved with a gain margin of 6 dB. Finally, it should be noted that the maximum stroke was kept below 2.7 cm when a chirp signal from 2 Hz to 9 Hz in duration of 600 seconds was used as excitation.

#### 5. Conclusions

This work studies the practical considerations to implement DVFC of vertical vibrations in pedestrian-bridge crossing. First of all, this work assumes the simplification of a second order system in order to show the maximum damping that can be imparted by a DVFC implemented with a real inertial mass actuator. The non-dimensional study shows that the maximum damping can be achieved when actuator natural frequency and the low cut-off frequency of the band-pass filter, which is used to implement the DVFC, are small enough. In addition, the frequency ratios are within a more restricted range when a higher gain margin is guaranteed. Secondly, the gain of the TFs that relates the force and stroke of the actuator with the excitation force are studied to show the influences of the aforementioned frequency ratios on the risk of force and stroke saturation. Thirdly, a practical guideline to design the band-pass filter for implementing DVFC is proposed. Fourthly, the model simplification, the design conclusions and a practical guideline are validated experimentally by implementing DVFC examples in a real light-weight steel-concrete composite structure (behaves similar to a footbridge). It is shown that for a civil structure with a fundamental vibration mode, the bandwidth of the filter and the gain margin of the controller are important design parameters to obtain a very good vibration attenuation performance, which is usually considered greater than or equal to 20 dB.

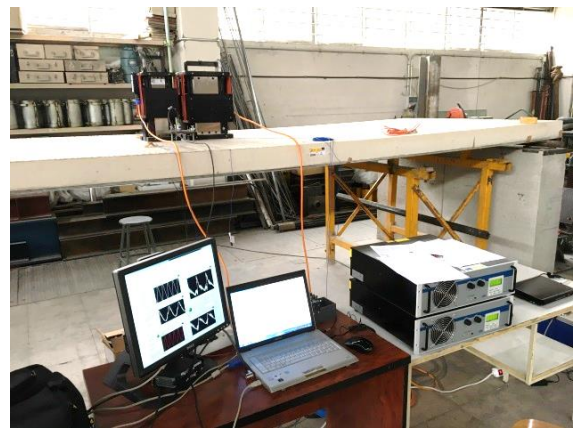
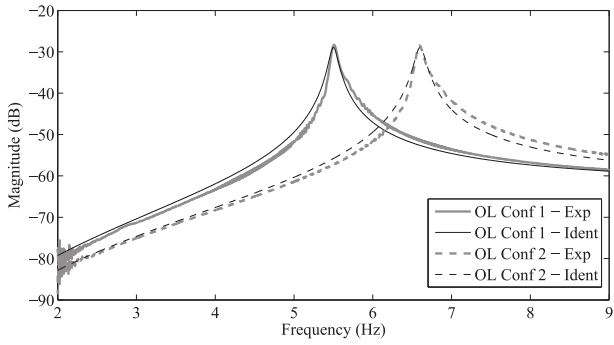
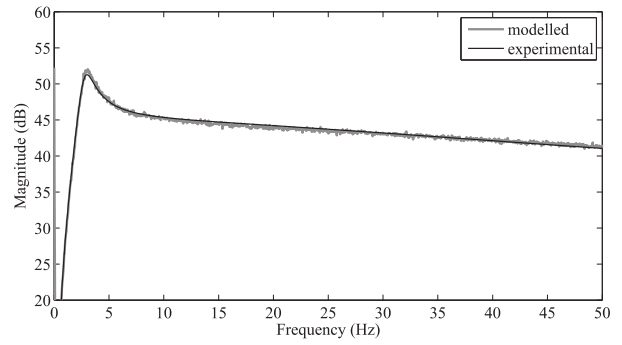


Fig. 10 Experimental SISO AVC implementation

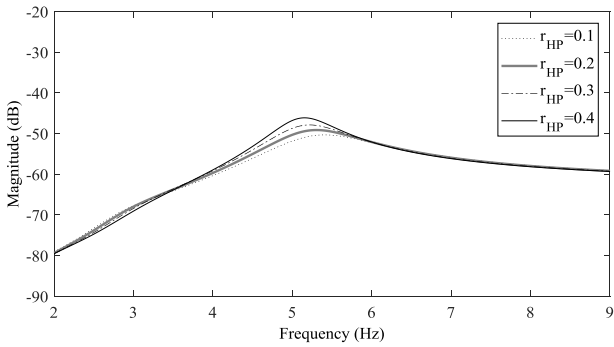


(a) structure configurations

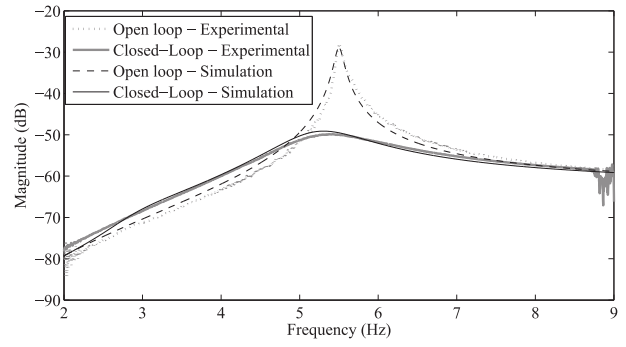


(b) controller actuator

Fig. 11 Experimental identifications

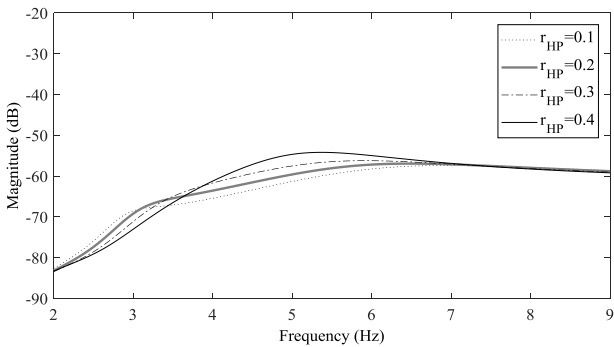


(a) FRFs of the closed-loop system in simulation when  $r_A = 0.49$  and gain margin equal to 12 dB

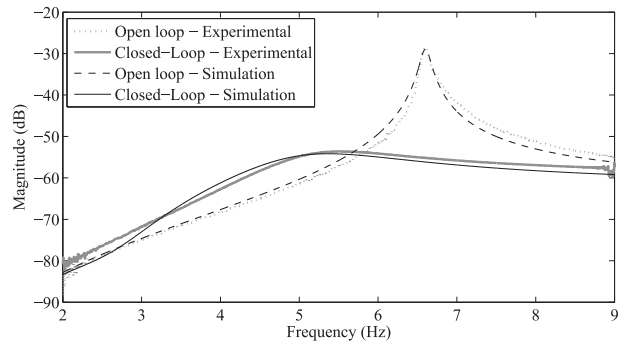


(b) comparison between experimental and simulation results when  $r_{HP} = 0.2$

Fig. 12 Experimental configuration 1



(a) FRFs of the closed-loop system in simulation when  $r_A = 0.41$  and gain margin equal to 6 dB



(b) comparison between experimental and simulation results when  $r_{HP} = 0.4$

Fig. 13 Experimental configuration 2.

## Acknowledgments

The work in this paper is part of the Spanish project DPI2013-47441-P: Development of new systems for reducing vibrations in pedestrian structures. The authors also acknowledge the partial financial support provided by the Research Net VIBRASTRUNET BIA2015-71942-REDT. One of the authors, Xidong Wang, wishes to thank China Scholarship Council (CSC) for financial assistance of a 4-year study at Universidad Politécnica de Madrid.

## References

- Alujevic, N., Zhao, G., Depraetere, B., Sas, P., Pluymers, B. and Desmet, W. (2014), "H2 optimal vibration control using inertial actuators and a comparison with tuned mass dampers", *J. Sound Vib.*, **333**(18), 4073-4083.
- Aphale, S.S., Fleming, A.J. and Moheimani, S.O.R. (2007), "Integral resonant control of collocated smart structures", *Smart Mater. Struct.*, **16**(2), 439-446.
- Bortoluzzi, D., Casciati, S., Elia, L. and Faravelli, L. (2014), "Design of a TMD solution to mitigate wind-induced local vibrations in an existing timber footbridge", *Smart Struct. Syst.*, **16**(3), 459-478.
- Casado, C.M., Díaz, I.M., de Sebastián, J., Poncela, A.V. and Lorenzana, A. (2013), "Implementation of passive and active vibration control on an in-service footbridge", *Struct. Control Health.*, **20**(1), 70-78.
- Casciati, F., Casciati, S. and Faravelli, L. (2017), "A contribution to the modelling of human induced excitation on pedestrian bridges", *Struct. Saf.*, **66**, 51-61.
- Casciati, S. (2016), "Human induced vibration vs. cable-stay footbridge deterioration", *Smart Struct. Syst.*, **18**(1), 17-29.
- Díaz, I.M. and Reynolds, P. (2009), "Robust saturated control of human-induced floor vibrations via a proof-mass actuator", *Smart Mater. Struct.*, **18**(12), 125024-125033.
- Díaz, I.M. and Reynolds, P. (2010), "Acceleration feedback control of human-induced floor vibrations", *Eng. Struct.*, **32**(1), 163-173.
- Díaz, I.M., Pereira, E. and Reynolds, P. (2012a), "Integral resonant control scheme for cancelling human-induced vibrations in light-weight pedestrian structures", *Struct. Control Health.*, **19**(1), 55-69.
- Díaz, I.M., Pereira, E., Hudson, M.J. and Reynolds, P. (2012b), "Enhancing active vibration control of pedestrian structures using inertial actuators with local feedback control", *Eng. Struct.*, **41**, 157-166.
- Griggs, W.M., Anderson, B.D.O. and Lanzon, A. (2007), "A 'mixed' small gain and passivity theorem in the frequency domain", *Syst. Control Lett.*, **56**(9-10), 596-602.
- Hanagan, L.M. (2005), "Walking-induced floor vibration case studies", *J. Archit. Eng.*, **11**(1), 14-18.
- Hudson, E.J., Reynolds, P. and Nyawako, D.S. (2016), "Fundamental studies of AVC with actuator dynamics", *Proceedings of the 34th IMAC Conference and Exposition on Structural Dynamics*, Orlando, USA, January.
- Hudson, M.J. and Reynolds, P. (2012), "Implementation considerations for active vibration control in the design of floor structures", *Eng. Struct.*, **44**, 334-358.
- Jang, D., Park, J. and Jung H. (2015), "Experimental investigation of an active mass damper system with time delay control algorithm", *Smart Struct. Syst.*, **15**(3), 863-879.
- Lu, X., Ding, K., Shi, W. and Weng, D. (2012), "Tuned mass dampers for human-induced vibration control of the Expo Culture Centre at the World Expo 2010 in Shanghai, China", *Struct. Eng. Mech.*, **43**(5), 607-621.
- Moutinho, C., Cunha, A. and Caetano, E. (2011), "Analysis and control of vibrations in a stress-ribbon footbridge", *Struct. Control Health.*, **18**(6), 619-634.
- Nagarajaiah, S. and Jung, H.J. (2014), "Smart tuned mass dampers: recent developments", *Smart Struct. Syst.*, **13**(2), 173-176.
- Nyawako, D., Reynolds P. and Hudson, E. (2016), "Incorporating a disturbance observer with direct velocity feedback for control of human-induced vibrations", *Proceedings of the SPIE 9799, Active and Passive Smart Structures and Integrated Systems*, Las Vegas, USA, April.
- Nyawako, D., Reynolds, P. and Hudson, E. (2015), "Dynamic compensators for floor vibration control", *Proceedings of the 33rd IMAC*, Orlando, USA, February.
- Ogata, K. (2010), *Modern Control Engineering*, Prentice Hall.
- Pereira, E. and Aphale, S.S. (2013), "Stability of positive-position feedback controllers with low-frequency restrictions", *J. Sound Vib.*, **332**(12), 2900-2999.
- Preumont, A. (2011), *Vibration Control of Active Structures*, (Third Edition), Springer.
- Soria, J.M., Díaz, I.M. and García-Palacios, J.H. (2017), "Vibration control of a time-varying modal-parameter footbridge: study of semi-active implementable strategies", *Smart Struct. Syst.*, **20**(5), 525-537.
- Teng, J., Xing, H.B., Xiao, Y.Q., Liu, C.Y., Li, H. and Ou J.P. (2014), "Design and implementation of AMD system for response control in tall buildings", *Smart Struct. Syst.*, **13**(2), 235-255.
- Ubaid, U., Daley, S. and Pope, S.A. (2015), "Design of remotely located and multi-loop vibration controllers using a sequential loop closing approach", *Control Eng. Pract.*, **38**, 1-10.
- Xu, H., Zhang, C., Li, H., Tan, P., Ou, J. and Zhou F. (2014), "Active mass driver control system for suppressing wind-induced vibration of the Canton Tower", *Smart Struct. Syst.*, **13**(2), 281-303.
- Zilletti, M. (2016), "Feedback control unit with an inerter proof-mass electrodynamic actuator", *J. Sound Vib.*, **369**, 16-28.
- Zilletti, M., Gardonio, P. and Elliott, S.J. (2014), "Optimisation of a velocity feedback controller to minimise kinetic energy and maximise power dissipation", *J. Sound Vib.*, **333**(19), 4405-4414.